HHS Public Access

Author manuscript

Pattern Recognit Lett. Author manuscript; available in PMC 2017 June 01.

Published in final edited form as:

Pattern Recognit Lett. 2016 June 1; 76: 83–89. doi:10.1016/j.patrec.2015.03.012.

In Vivo Precision of Digital Topological Skeletonization Based Individual Trabecula Segmentation (ITS) Analysis of Trabecular Microstructure at the Distal Radius and Tibia by HR-pQCT

Bin Zhou[a], **Zhendong Zhang**[a,b], **Ji Wang**[a], **Y. Eric Yu**[a], **Xiaowei Sherry Liu**[a,c], **Kyle K. Nishiyama**[d], **Mishaela R. Rubin**[d], **Elizabeth Shane**[d], **John P. Bilezikian**[d], and **X. Edward Guo**[a,*]

[a]Bone Bioengineering Laboratory, Department of Biomedical Engineering, Columbia University, New York, New York, U.S.A.

[b]Department of Orthopedic Surgery, First Affiliated Hospital, School of Medicine, Shihezi University, Shihezi, Xinjiang, China.

[c]McKay Orthopaedic Research Laboratory, Department of Orthopaedic Surgery, University of Pennsylvania, Philadelphia, PA, U.S.A.

[d]Division of Endocrinology, Department of Medicine, Columbia University, New York, New York, U.S.A.

Abstract

Trabecular plate and rod microstructure plays a dominant role in the apparent mechanical properties of trabecular bone. With high-resolution computed tomography (CT) images, digital topological analysis (DTA) including skeletonization and topological classification was applied to transform the trabecular three-dimensional (3D) network into surface and curve skeletons. Using the DTA-based topological analysis and a new reconstruction/recovery scheme, individual trabecula segmentation (ITS) was developed to segment individual trabecular plates and rods and quantify the trabecular plate- and rod-related morphological parameters. High-resolution peripheral quantitative computed tomography (HR-pQCT) is an emerging *in vivo* imaging technique to visualize 3D bone microstructure. Based on HR-pQCT images, ITS was applied to various HR-pQCT datasets to examine trabecular plate- and rod-related microstructure and has demonstrated great potential in cross-sectional and longitudinal clinical applications. However, the reproducibility of ITS has not been fully determined. The aim of the current study is to quantify the precision errors of ITS plate-rod microstructural parameters. In addition, we utilized three different frequently used contour techniques to separate trabecular and cortical bone and to evaluate their effect on ITS measurements.

[*]Corresponding author. Tel.: +001-212-854-6196; fax: +001-212-854-8725; exg1@columbia.edu; address: 351 Engineering Terrace, 1210 Amsterdam Avenue, New York, NY 10027, U.S.A..

Conflict of Interest

The authors declare that there are no conflicts of interest regarding the submitted manuscript

Overall, good reproducibility was found for the standard HR-pQCT parameters with precision errors for volumetric BMD and bone size between 0.2%-2.0%, and trabecular bone microstructure between 4.9%-6.7% at the radius and tibia. High reproducibility was also achieved for ITS measurements using all three different contour techniques. For example, using automatic contour technology, low precision errors were found for plate and rod trabecular number (pTb.N, rTb.N, 0.9% and 3.6%), plate and rod trabecular thickness (pTb.Th, rTb.Th, 0.6% and 1.7%), plate trabecular surface (pTb.S, 3.4%), rod trabecular length (rTb.ℓ, 0.8%), and plate-plate junction density (P-P Junc.D, 2.3%) at the tibia. The precision errors at the radius were similar to those at the tibia. In addition, precision errors were affected by the contour technique. At the tibia, precision error by the manual contour method was significantly different from automatic and standard contour methods for pTb.N, rTb.N and rTb.Th. Precision error using the manual contour method was also significantly different from the standard contour method for rod trabecular number (rTb.N), rod trabecular thickness (rTb.Th), rod-rod and plate-rod junction densities (R-R Junc.D and P-R Junc.D) at the tibia. At the radius, the precision error was similar between the three different contour methods. Image quality was also found to significantly affect the ITS reproducibility. We concluded that ITS parameters are highly reproducible, giving assurance that future cross-sectional and longitudinal clinical HR-pQCT studies are feasible in the context of limited sample sizes.

Keywords

Individual trabecular segmentation (ITS); HR-pQCT; precision error; trabecular microstructure; osteoporosis

1. Introduction

Three-dimensional (3D) skeletonization is an important technique for characterizing and quantifying complex 3D microstructures. Digital topological analysis (DTA) is a powerful skeletonization and classification technique that preserves microstructural topology. It was developed by Saha et al. and has been applied in analyzing the 3D microstructure of objects including human trabecular bone (Gomberg et al., 2000; Saha and Chaudhuri, 1994, 1996; Saha et al., 1994). Osteoporosis is a serious metabolic bone disease characterized by reduced bone mass, impaired trabecular bone microstructure and increased fracture risk. DTA-based parameters, such as the ratio of surface (plate-like) to curve (rod-like) microstructural elements and erosion ratio, were important in characterizing trabecular bone microstructure. Based on DTA-skeletonization and classification, we further developed an individual trabecula segmentation (ITS) technique using skeleton breakages and volume-preserving reconstruction/recovery, where the entire 3D trabecular bone microstructure was decomposed into a collection of individual trabecular plates and rods (Liu et al., 2008). ITS has been applied to both micro computed tomography (μCT) and clinical high-resolution peripheral quantitative computed tomography (HR-pQCT) images for quantification of trabecular bone microstructure (Liu et al., 2010a; Sutter et al., 2014; Walker et al., 2013; Wang et al., 2013; Zhou et al., 2014a; Zhou et al., 2014b). Independent of DXA, HR-pQCT-based ITS measurements can distinguish among postmenopausal women with and without a history of fragility fracture (Liu et al., 2012). Furthermore, we have demonstrated that

trabecular plate differences as detected by ITS analysis primarily account for the differences in mechanical properties between Chinese-American and Caucasian women (Liu et al., 2011b). Most recently, we also demonstrated that depletion of trabecular plates results in significantly reduced bone strength in patients with primary hyperparathyroidism (Stein et al., 2013).

HR-pQCT, an emerging imaging modality, demonstrates potential to quantitate bone quality through noninvasive 3D visualization of cortical and trabecular bone microstructure. HR-pQCT provides quantitative measures of volumetric bone mineral density (*v*BMD), bone geometry and bone microstructural parameters (Boutroy et al., 2005). Furthermore, HR-pQCT helps to capture the minor changes in bone microstructure that can not be observed by DXA (Jn et al., 2014; Nishiyama et al., 2014). Studies using HR-pQCT have demonstrated that changes in trabecular bone microstructure are associated with significant reductions in bone strength (Boutroy et al., 2008; Cohen et al., 2009; Melton et al., 2007; Yin et al., 2013). For example, patients with a history of fracture were found to have fewer and thinner trabeculae, resulting in significantly lower bone stiffness (Nishiyama et al., 2013; Sornay-Rendu et al., 2007).

Three different segmentation methods have been adopted in the literature to separate trabecular bone from cortical bone for bone microstructural analysis of HR-pQCT: 1) automated segmentation, which uses two threshold values and a series of dilation and erosion operations to extract the endosteal surface of the cortex, which separates the trabecular bone from cortical bone (Burghardt et al., 2010; Nishiyama et al., 2010); 2) manual contouring through visual inspection on each slice of the 3D bone image to manually define the boundary between the trabecular and cortical bone (Liu et al., 2010b); 3) standard contouring provided by the manufacturer, which separates trabecular from cortical bone through bone mineral density-based assumptions (Boutroy et al., 2005; Laib et al., 1998). It is not clear whether ITS analyzed plate/rod parameters would be affected differently by these three methods.

The accuracy of HR-pQCT image-based ITS measurements has been evaluated through comparison with high resolution micro computed tomography (μCT) images (Liu et al., 2011a). However, to better interpret HR-pQCT-based ITS morphological parameters in longitudinal studies, data related to its reproducibility needs to be assessed. The objective of this study is to determine the precision error of HR-pQCT-based ITS analysis. In addition, we examined the precision errors among all three cortical-trabecular segmentation methods.

2. Materials and Methods

2.1 Individual Trabecula Segmentation (ITS)-Based Morphological Analyses of HR-pQCT Images

ITS was applied to the trabecular compartment to evaluate the plate/rod related microstructural parameters (Liu et al., 2008; Liu et al., 2006). The characterization of trabecular plate and rod was accomplished through digital topological analysis of the binarized trabecular bone image based on the theory and algorithm developed by Saha et al, which includes skeletonization and topological classification of the trabecular bone network

(Gomberg et al., 2000; Saha and Chaudhuri, 1994, 1996; Saha et al., 1994; Saha et al., 1997). Skeletonization is an iterative erosion process where bone voxels are peeled off layer by layer until no further bone voxels can be removed without changing the shape of the trabecular microarchitecture, transforming trabecular bone into a representation composed of surface and curves while preserving the topology (Fig. 1). The iteration number, representing the depth of the layer, was recorded for each voxel at the time of its removal (Saha and Chaudhuri, 1994; Saha et al., 1994). After skeletonization, digital topological classification is applied to identify each bone voxel as surface or curve type. The method of topological classification was based on the number of objects, tunnels, and cavities in the 3×3×3 neighborhood of a bone voxel after the latter's hypothetical transformation to a marrow voxel (Saha and Chaudhuri, 1996). These topological characteristics of a bone voxel led to an unambiguous determination of its topological classes, e.g. surface, curve, edge, and junctions (Fig. 1B). The surface skeletons were further processed into arc skeletons (Fig. 1C). The arc-curve or curve-curve junction points were used to split the skeleton into individual segments. Each segment was labeled with a unique identity number and its topological marker as either a trabecular rod or a plate skeleton. Then, volumetric reconstruction of each individual trabecular plate and rod was accomplished by an iterative topological marking of nonskeletal voxels starting from the skeletal voxels (Liu et al., 2006). During the reverse filling process, the trabecular plate and rod skeleton was dilated also in a layer-by-layer fashion until fully reconstructed to the original volume. On completion of the reconstruction process, each bone voxel was labeled as belonging to an individual trabecular plate or rod (Fig. 1D). Based on the complete decomposition of the trabecular bone network, the following parameters were evaluated: plate and rod bone volume fraction (pBV/TV and rBV/TV); plate and rod number density (pTb.N and rTb.N, 1/mm); axial bone volume fraction (aBV/TV); plate and rod trabecular thickness (pTb.Th and rTb.Th, mm); plate trabecular surface (pTb.S, mm^2) and rod trabecular length (rTb.ℓ, mm); trabecular connection densities between plate-plate, plate-rod and rod-rod (P-P Junc.D, P-R Junc.D and R-R Junc.D, $1/mm^3$). A direct measure of bone volume fraction (BV/TV), voxels occupied by bone divided by total voxels, was also reported, as the parameter reported by HR-pQCT is derived rather than measured directly.

2.2 Study Population and HR-pQCT Scanning

Thirty community dwelling subjects were recruited at Columbia University Medical Center by advertisement, self-referral or physician referral (age 45±14 years, 7 male/23 female). All subjects provided written informed consent, and the Institutional Review Boards of Columbia University Medical Center approved this study. HR-pQCT scans were performed twice within a 48-hour interval. The non-dominant forearm and corresponding distal tibia were scanned by HR-pQCT (XtremeCT, Scanco Medical, Brüttisellen, Switzerland). The HR-pQCT measurement included 110 slices, corresponding to a 9.02 mm section along the axial direction, with an isotropic voxel size of 82 μm. Quality control was provided by scanning the European Forearm Phantom at the time subjects were scanned. The mineralized phase was thresholded according to the standard patient evaluation protocol (Laib et al., 1998).

To segment the trabecular compartment from the whole bone image and prepare for ITS analysis, three frequently used segmentation methods were applied to investigate their influence on ITS reproducibility. An automatic segmentation algorithm (auto contour) implemented in Image Processing Language (IPL V5.07, Scanco Medical, Switzerland) was used to automatically segment the trabecular bone from whole bone (Fig. 2A). Manual contouring was performed based on the thresholded image after the standard HR-pQCT evaluation, by visual inspections to manually define the boundary (manual contour) separating the trabecular and cortical bone, which is considered the gold-standard method (Fig. 2B). For the third method (standard), based on the standard HR-pQCT segmentation technique, the entire bone region was automatically separated into cortical and trabecular compartments using a threshold-based algorithm (Fig. 2C). The resulting trabecular bone volumes from auto, manual and standard cortical-trabecular segmentation techniques are shown in Figures 2D, E, and F, respectively.

To examine the effect of image quality on ITS measurements, each scan was given a grade based on inspection of three slices (distal, middle and proximal). Five different grades from 1 (no motion artifact) to 5 (severe motion artifact) were used to quantify the image quality according to the manufacturer's recommendations. Three trained technicians carried out the image grading and a consensus grade would be determined if the grades were different between graders. The scans were then categorized into two image quality groups to examine their effect: grade 1 group (G1) includes subjects for whom both scans were given grade 1. Those whose scans received a grade of 2, 3, or 4 were categorized as G2-4. No scan was characterized as grade 5.

2.3 Statistical Analysis

Mean and standard deviation were used to characterize the ITS parameters from two scan time points for both the radius and tibia. The HR-pQCT and ITS precision errors were calculated as root mean square coefficient of variation (RMSCV) for pooled data and for data categorized with different motion grade levels, respectively (Gluer et al., 1995). Student *t*-test was used to examine the precision error difference between different grade levels. Repeated analysis of variance (ANOVA) was performed to examine the precision error difference between the three contour methods (NCSS 2007, NCSS Statistical Software, Kaysville, UT, USA). In order to quantify the changes detectable in longitudinal studies, least significant detectable change was also calculated based on following the formula (Shepherd and Lu, 2007): LSC = 2.77 × precision error

3. Results

The mean percentage of the common region between first and follow up scans was 95% for the tibia and 90% for the radius. The average follow up scan occurred within 24 hours after the first scan. The scans at the tibia had better image quality than the radius, with 22 subjects categorized as grade 1 and the remaining 8 as grade 2 or 3. There were no subjects who were scored grade 4. The radius was more prone to be influenced by motion artifact as evidenced by 7 subjects who were categorized as grade 1, 19 subjects as grade 2 or 3 and 5 subjects categorized as grade 4.

The precision errors for standard HR-pQCT evaluated parameters are shown in Table 1. In general, all HR-pQCT measurements were highly reproducible. The precision error for volumetric bone mineral density and bone area was less than 2% at the radius and tibia. Trabecular bone microstructural parameters had relatively higher precision errors ranging between 4.9% and 6.7%. The mean and standard deviation for ITS measured plate- and rod-related parameters are shown in Table 2 with the three different contour techniques. Significant differences existed for ITS parameters using the three techniques. At the tibia, the plate and rod trabecular number (pTb.N and rTb.N), rod trabecular thickness (rTb.Th), plate-plate and rod-rod junction density (P-P and R-R Junc.D) using the automatic contour method were all significantly higher than the other two methods ($p<0.05$). At the radius, the differences were similar to the tibia, with plate and rod bone volume fraction (pBV/TV and rBV/TV) also significantly higher in ITS evaluations using the automatic contour method ($p<0.05$).

The precision errors for ITS evaluations are shown in Table 3 with data pooled together and further categorized as grade 1 (G1) and grades 2, 3 or 4 (G2-4) for the three contour methods. Overall the data were highly reproducible, with most precision errors less than 7%. pTb.N, pTb.Th, rTb.Th and rTb.ℓ had lower precision errors than the rest of the ITS parameters, with the precision error less than 2% at the radius and tibia. Rod-rod junction density (R-R Junc.D) had the highest precision error (>10%). At the tibia, the precision errors of rTb.N and rTb.Th were slightly higher in the manual contour group than the automatic contour and standard contour group ($p<0.05$). In addition, P-R and R-R junction densities were also found to be significantly higher in the manual contour group than the standard contour group. At the radius, there were no differences found between the three different contour groups. The ITS reproducibility was greatly affected by the image quality grade. Significant differences between G1 and G2-4 groups were found for most ITS parameters at the tibia using all three contour methods. At the radius, G1 and G2-4 groups were also found to be significantly different in the manual contour group. The least significant changes for both the radius and tibia are shown in Table 4. In accordance with the precision error, the minimum change that can be detectable between two scans was lowest in plate and rod trabecular thickness and highest in rod-rod junction density.

4. Discussion

ITS has been shown to be an effective morphological evaluation technique that provides independent measurements of trabecular plate- and rod-related microstructural parameters. ITS has demonstrated its great potential in clinical studies to evaluate disease and treatment-related bone microstructural changes (Liu et al., 2010a; Liu et al., 2012; Liu et al., 2011b; Nishiyama et al., 2014; Yin et al., 2013; Zhou et al., 2014b). In this study, we quantified the precision errors of ITS using HR-pQCT scans of 30 subjects at the distal radius and tibia. Based on the skeletonization and topological classification of the trabecular 3D microstructure, the trabecular network was completely decomposed into individual trabecular plate and rod elements. We determined the reproducibility of HR-pQCT based ITS measurements with three different segmentation methods. The influence of image quality on the ITS reproducibility was also examined. This precision study provides important reference data for future cross-sectional and longitudinal HR-pQCT studies.

Trabecular microstructure derived by standard HR-pQCT evaluations are model dependent parameters with the trabecular number as the only independently calculated parameter, whereas other trabecular microstructural parameters such as trabecular separation and trabecular thickness are derived from trabecular number (Boutroy et al., 2005). In contrast, ITS calculates trabecular plate and rod related parameters independently, such as the plate and rod thickness, plate and rod number, plate surface and rod length, providing more detailed evaluations of bone microstructure.

The precision errors of the standard HR-pQCT measurements in our study are comparable to previous reports. Engelke et al. evaluated HR-pQCT short-term in vivo reproducibility and reported 6.24% and 5.94% precision errors for Tb.N and Tb.Th (Engelke et al., 2012). In addition, after excluding images with motion artifacts, MacNeil et al. reported 3.6% and 3.41% precision errors for Tb.N and Tb.Th at the distal radius and similar precision errors at the tibia assessed by standard HR-pQCT analyses (MacNeil and Boyd, 2008). The ITS precision errors in current study are comparable to the traditional parameters by standard HR-pQCT evaluations, for example, precision errors for pTb.N and pTb.Th at the tibia were 1.53% and 0.22%. The small ITS precision errors resulted in minor least significant detectable changes, with the detectable changes for plate trabecular thickness, rod trabecular thickness, rod trabecular length less than 15 μm, which is less than half of the HR-pQCT voxel size.

The precision errors varied among ITS parameters, with plate and rod trabecular thickness, plate trabecular surface and rod trabecular length smaller than other parameters. The least significant detectable changes provide boundaries to quantify the trabecular microstructural differences using ITS. For example, with ITS analysis, we observed the absolute difference between Chinese-American and Caucasian women was 0.22 (1/mm) for trabecular plate number and 0.02 (mm) for trabecular plate thickness at the radius (Liu et al., 2011b), which were significantly higher than the detectable changes suggested in this study.

In this study, we determined the reproducibility of ITS parameters with different segmentation techniques. We found that the ITS results varied using different segmentation techniques, especially for plate and rod trabecular number. The difference can be close to 2% for plate trabecular number and 0.8% for rod trabecular number when comparing the manual contour group to the automatic contour group. The result suggests that one single contour method should be used consistently within a cross-sectional study or longitudinal study, and that a mix of contour methods could introduce significant errors. In this study, we also examined the influence of motion artifacts on the ITS precision errors. The results showed that there was a significant motion effect on the ITS reproducibility. The precision error can be doubled due to motion artifacts, highlighting the importance of minimizing the motion in the scanning process in future clinical studies. Compared with the precision errors at the tibia, the radius was found to have higher precision errors. This is primarily due to the higher motion artifact observed in radius scans. The number of radius scans was close to 3 times the number of tibia scans that were categorized as quality grade 2, 3 or 4. In addition, most tibia scans were categorized as grade 2, while half of the radius scans were categorized as grade 3 or 4.

In conclusion, ITS analysis shows high reproducibility for evaluating trabecular bone microstructure based on HR-pQCT scans. The influence of different contour techniques and motion artifacts on ITS precision errors was also quantified. This study provides guidelines for the application of ITS in cross-sectional and longitudinal studies to better understand trabecular microstructural changes.

Acknowledgements

This work was partially supported by grants from National Institutes of Health (AR051376, AR058004, DK069350, DK32333).

References

Boutroy S, Bouxsein ML, Munoz F, Delmas PD. In vivo assessment of trabecular bone microarchitecture by high-resolution peripheral quantitative computed tomography. J Clin Endocrinol Metab. 2005; 90:6508–6515. [PubMed: 16189253]

Boutroy S, Van Rietbergen B, Sornay-Rendu E, Munoz F, Bouxsein ML, Delmas PD. Finite element analysis based on in vivo HR-pQCT images of the distal radius is associated with wrist fracture in postmenopausal women. J Bone Miner Res. 2008; 23:392–399. [PubMed: 17997712]

Burghardt AJ, Kazakia GJ, Ramachandran S, Link TM, Majumdar S. Age- and gender-related differences in the geometric properties and biomechanical significance of intracortical porosity in the distal radius and tibia. J Bone Miner Res. 2010; 25:983–993. [PubMed: 19888900]

Cohen A, Liu XS, Stein EM, McMahon DJ, Rogers HF, Lemaster J, Recker RR, Lappe JM, Guo XE, Shane E. Bone microarchitecture and stiffness in premenopausal women with idiopathic osteoporosis. J Clin Endocrinol Metab. 2009; 94:4351–4360. [PubMed: 19837923]

Engelke K, Stampa B, Timm W, Dardzinski B, de Papp AE, Genant HK, Fuerst T. Short-term in vivo precision of BMD and parameters of trabecular architecture at the distal forearm and tibia. Osteoporos Int. 2012; 23:2151–2158. [PubMed: 22143491]

Gluer CC, Blake G, Lu Y, Blunt BA, Jergas M, Genant HK. Accurate assessment of precision errors: how to measure the reproducibility of bone densitometry techniques. Osteoporos Int. 1995; 5:262–270. [PubMed: 7492865]

Gomberg BR, Saha PK, Song HK, Hwang SN, Wehrli FW. Topological analysis of trabecular bone MR images. Ieee T Med Imaging. 2000; 19:166–174.

Jn T, Av U, Sm BB, Rm N, Y Z, N D, H L, Ml B, Bz L. Comparative Effects of Teriparatide, Denosumab, and Combination Therapy on Peripheral Compartmental Bone Density, Microarchitecture, and Estimated Strength: the DATA-HRpQCT Study. J Bone Miner Res. 2014

Laib A, Hauselmann HJ, Ruegsegger P. In vivo high resolution 3D-QCT of the human forearm. Technol Health Care. 1998; 6:329–337. [PubMed: 10100936]

Liu XS, Cohen A, Shane E, Stein E, Rogers H, Kokolus SL, Yin PT, McMahon DJ, Lappe JM, Recker RR, Guo XE. Individual trabeculae segmentation (ITS)-based morphological analysis of high-resolution peripheral quantitative computed tomography images detects abnormal trabecular plate and rod microarchitecture in premenopausal women with idiopathic osteoporosis. J Bone Miner Res. 2010a; 25:1496–1505. [PubMed: 20200967]

Liu XS, Sajda P, Saha PK, Wehrli FW, Bevill G, Keaveny TM, Guo XE. Complete volumetric decomposition of individual trabecular plates and rods and its morphological correlations with anisotropic elastic moduli in human trabecular bone. J Bone Miner Res. 2008; 23:223–235. [PubMed: 17907921]

Liu XS, Sajda P, Saha PK, Wehrli FW, Guo XE. Quantification of the roles of trabecular microarchitecture and trabecular type in determining the elastic modulus of human trabecular bone. J Bone Miner Res. 2006; 21:1608–1617. [PubMed: 16995816]

Liu XS, Shane E, McMahon DJ, Guo XE. Individual trabecula segmentation (ITS)-based morphological analysis of microscale images of human tibial trabecular bone at limited spatial resolution. J Bone Miner Res. 2011a; 26:2184–2193. [PubMed: 21557311]

Liu XS, Stein EM, Zhou B, Zhang CA, Nickolas TL, Cohen A, Thomas V, McMahon DJ, Cosman F, Nieves J, Shane E, Guo XE. Individual trabecula segmentation (ITS)-based morphological analyses and microfinite element analysis of HR-pQCT images discriminate postmenopausal fragility fractures independent of DXA measurements. J Bone Miner Res. 2012; 27:263–272. [PubMed: 22072446]

Liu XS, Walker MD, McMahon DJ, Udesky J, Liu G, Bilezikian JP, Guo XE. Better skeletal microstructure confers greater mechanical advantages in Chinese-American women versus white women. J Bone Miner Res. 2011b; 26:1783–1792. [PubMed: 21351150]

Liu XS, Zhang XH, Sekhon KK, Adams MF, McMahon DJ, Bilezikian JP, Shane E, Guo XE. High-resolution peripheral quantitative computed tomography can assess microstructural and mechanical properties of human distal tibial bone. J Bone Miner Res. 2010b; 25:746–756. [PubMed: 19775199]

MacNeil JA, Boyd SK. Improved reproducibility of high-resolution peripheral quantitative computed tomography for measurement of bone quality. Med Eng Phys. 2008; 30:792–799. [PubMed: 18164643]

Melton LJ 3rd, Riggs BL, van Lenthe GH, Achenbach SJ, Muller R, Bouxsein ML, Amin S, Atkinson EJ, Khosla S. Contribution of in vivo structural measurements and load/strength ratios to the determination of forearm fracture risk in postmenopausal women. J Bone Miner Res. 2007; 22:1442–1448. [PubMed: 17539738]

Nishiyama KK, Cohen A, Young P, Wang J, Lappe JM, Guo XE, Dempster DW, Recker RR, Shane E. Teriparatide increases strength of the peripheral skeleton in premenopausal women with idiopathic osteoporosis: A pilot HR-pQCT study. J Clin Endocrinol Metab. 2014:jc20141041.

Nishiyama KK, Macdonald HM, Buie HR, Hanley DA, Boyd SK. Postmenopausal women with osteopenia have higher cortical porosity and thinner cortices at the distal radius and tibia than women with normal aBMD: an in vivo HR-pQCT study. J Bone Miner Res. 2010; 25:882–890. [PubMed: 19839766]

Nishiyama KK, Macdonald HM, Hanley DA, Boyd SK. Women with previous fragility fractures can be classified based on bone microarchitecture and finite element analysis measured with HR-pQCT. Osteoporos Int. 2013; 24:1733–1740. [PubMed: 23179565]

Saha PK, Chaudhuri BB. Detection of 3-D Simple Points for Topology Preserving Transformations with Application to Thinning. Ieee T Pattern Anal. 1994; 16:1028–1032.

Saha PK, Chaudhuri BB. 3D digital topology under binary transformation with applications. Comput Vis Image Und. 1996; 63:418–429.

Saha PK, Chaudhuri BB, Chanda B, Majumder DD. Topology Preservation in 3d Digital Space. Pattern Recogn. 1994; 27:295–300.

Saha PK, Chaudhuri BB, Dutta D, Majumder DD. A new shape preserving parallel thinning algorithm for 3D digital images. Pattern Recogn. 1997; 30:1939–1955.

Shepherd JA, Lu Y. A generalized least significant change for individuals measured on different DXA systems. J Clin Densitom. 2007; 10:249–258. [PubMed: 17616413]

Sornay-Rendu E, Boutroy S, Munoz F, Delmas PD. Alterations of cortical and trabecular architecture are associated with fractures in postmenopausal women, partially independent of decreased BMD measured by DXA: the OFELY study. J Bone Miner Res. 2007; 22:425–433. [PubMed: 17181395]

Stein EM, Silva BC, Boutroy S, Zhou B, Wang J, Udesky J, Zhang C, McMahon DJ, Romano M, Dworakowski E, Costa AG, Cusano N, Irani D, Cremers S, Shane E, Guo XE, Bilezikian JP. Primary hyperparathyroidism is associated with abnormal cortical and trabecular microstructure and reduced bone stiffness in postmenopausal women. J Bone Miner Res. 2013; 28:1029–1040. [PubMed: 23225022]

Sutter S, Nishiyama KK, Kepley A, Zhou B, Wang J, McMahon DJ, Guo XE, Stein EM. Abnormalities in Cortical Bone, Trabecular Plates, and Stiffness in Postmenopausal Women Treated With Glucocorticoids. J Clin Endocr Metab. 2014; 99:4231–4240. [PubMed: 25127089]

Walker MD, Liu XS, Zhou B, Agarwal S, Liu G, McMahon DJ, Bilezikian JP, Guo XE. Premenopausal and postmenopausal differences in bone microstructure and mechanical competence in Chinese-American and white women. J Bone Miner Res. 2013; 28:1308–1318. [PubMed: 23299863]

Wang J, Zhou B, Parkinson I, Thomas CDL, Clement JG, Fazzalari N, Guo XE. Trabecular Plate Loss and Deteriorating Elastic Modulus of Femoral Trabecular Bone in Intertrochanteric Hip Fractures. Bone Research. 2013; 4:346–354. [PubMed: 26273512]

Yin MT, Lund E, Shah J, Zhang CA, Foca M, Neu N, Nishiyama KK, Zhou B, Guo XE, Nelson J, Bell DL, Shane E, Arpadi SM. Lower peak bone mass and abnormal trabecular and cortical microarchitecture in young men infected with HIV early in life. AIDS. 2013

Zhou B, Liu XS, Wang J, Lu XL, Fields AJ, Guo XE. Dependence of mechanical properties of trabecular bone on plate-rod microstructure determined by individual trabecula segmentation (ITS). J Biomech. 2014a; 47:702–708. [PubMed: 24360196]

Zhou B, Wang J, Stein EM, Zhang Z, Nishiyama KK, Zhang CA, Nickolas TL, Shane E, Guo XE. Bone density, microarchitecture and stiffness in Caucasian and Caribbean Hispanic postmenopausal American women. Bone Research. 2014b; 2:14016. [PubMed: 26273525]

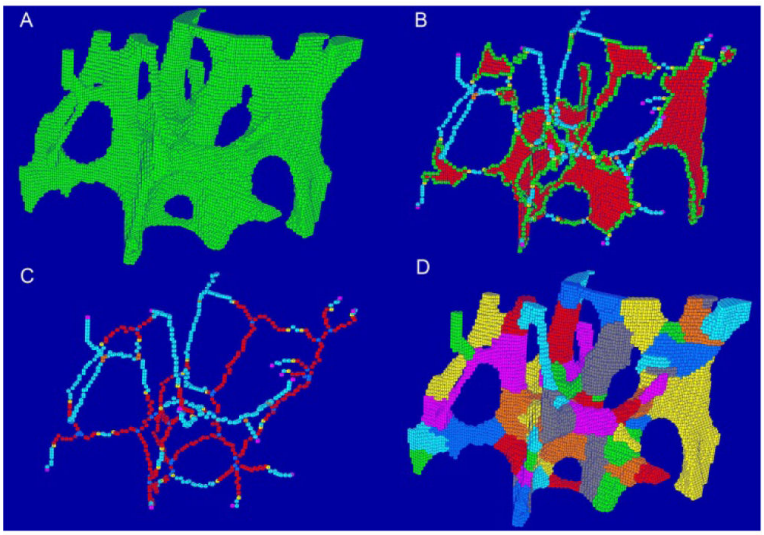

Figure 1.

Illustration of the digital topological skeletonization and classification based complete volumetric decomposition of human trabecular bone. (A) An original trabecular bone image from proximal tibia. (B) Skeletonization and topological classification of trabecular bone. (C) Arc thinning and plate topological classification, (D) Complete reconstruction of trabecular bone, with different color represents individual trabecular.

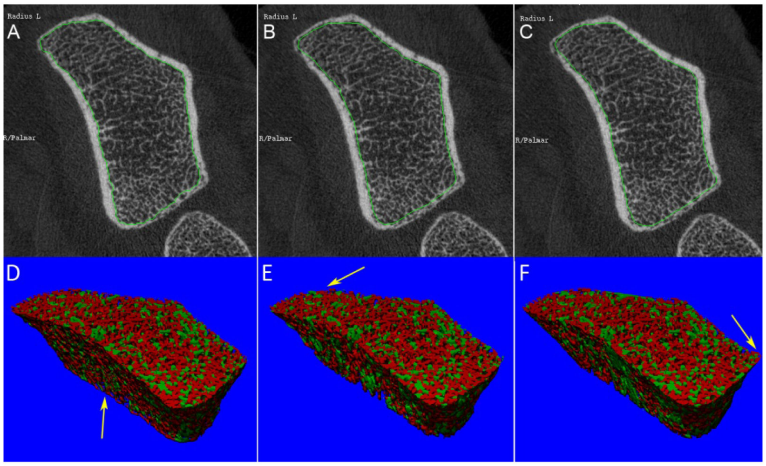

Figure 2.

Demonstration of the contouring techniques used to separate trabecular bone from cortical bone, contours in green. (A) Contours using automatic contouring method. (B) Contours generated manually. (C) Contours generating based on the standard segmentation. (D-F) The corresponding trabecular plate and rod related microstructure by ITS based on the contouring methods in (A-C). Red represents trabecular rod and green represents trabecular plate. Arrow indicates the differences compared to the other two images.

Table 1

Root mean square coefficient of variance (RMSCV%) of the standard HR-pQCT measurements

Average common region	Tibia	Radius
	95%	90%
Cortical area (mm^2)	1.2	2.0
Trabecular area (mm^2)	0.2	0.56
Average BMD ($mgHA/cm^3$)	1.2	1.2
Cortical BMD ($mgHA/cm^3$)	0.9	1.26
Cortical thickness (mm)	1.3	2.45
Trabecular BMD ($mgHA/cm^3$)	1.3	1.56
Trabecular number (1/mm)	5.3	6.5
Trabecular thickness (mm)	4.9	6
Trabecular separation (mm)	5.4	6.7

Table 2

Summary of quantitative ITS measures for radius and tibia. S1 represent first scan, S2 represent the following scan.

	Auto Contour S1	Auto Contour S2	Manual S1	Manual S2	Standard S1	Standard S2
Tibia						
BV/TV	0.309±0.053	0.31±0.052	0.305±0.055	0.306±0.054	0.286±0.047 *,†	0.286±0.047 *,†
pBV/TV	0.136±0.054	0.138±0.057	0.133±0.056	0.135±0.058	0.118±0.045 *,†	0.119±0.045 *,†
rBV/TV	0.173±0.045	0.171±0.045	0.172±0.045	0.17±0.045	0.168±0.044 *,†	0.167±0.043 *,†
aBV/TV	0.128±0.038	0.13±0.04	0.127±0.04	0.129±0.041	0.114±0.032 *,†	0.115±0.032 *,†
pBV/BV	0.436±0.131	0.44±0.131	0.429±0.134	0.435±0.134	0.409±0.125 *,†	0.413±0.124 *,†
rBV/BV	0.564±0.131	0.56±0.131	0.571±0.134	0.565±0.134	0.591±0.125 *,†	0.587±0.124 *,†
pTb.N (1/mm)	1.531±0.151	1.534±0.149	1.513±0.161 *	1.517±0.156 *	1.512±0.154 *	1.516±0.153 *
rTb.N (1/mm)	1.903±0.216	1.894±0.214	1.888±0.222 *	1.878±0.22 *	1.915±0.207 *,†	1.907±0.201 *,†
pTb.Th (mm)	0.222±0.01	0.222±0.011	0.222±0.011	0.222±0.011	0.212±0.008 *,†	0.212±0.008 *,†
rTb.Th (mm)	0.212±0.006	0.213±0.007	0.214±0.007 *	0.215±0.007 *	0.208±0.006 *,†	0.208±0.007 *,†
pTb.S (mm^2)	0.162±0.021	0.163±0.021	0.163±0.021	0.164±0.021	0.153±0.016 *,†	0.153±0.015 *,†
rTb.ℓ (mm)	0.644±0.027	0.643±0.025	0.645±0.028	0.644±0.027	0.639±0.025 *,†	0.638±0.024 *,†
R-R Junc.D ($1/mm^3$)	3.098±1.284	3.049±1.311	3.043±1.297 *	2.993±1.321 *	3.174±1.238 *,†	3.122±1.248 *,†
R-P Junc.D ($1/mm^3$)	4.496±1.099	4.455±1.015	4.365±1.122	4.329±1.034 *	4.522±1.139 *,†	4.49±1.028 †
P-P Junc.D ($1/mm^3$)	2.388±0.602	2.398±0.586	2.318±0.629 *	2.33±0.603 *	2.326±0.6 *	2.344±0.592 *
Radius						
BV/TV	0.282±0.071	0.284±0.072	0.275±0.074 *	0.277±0.076 *	0.258±0.068 *,†	0.259±0.068 *,†
pBV/TV	0.098±0.051	0.097±0.054	0.093±0.053 *	0.092±0.056 *	0.084±0.045 *,†	0.083±0.047 *,†
rBV/TV	0.185±0.041	0.188±0.044	0.182±0.042 *	0.184±0.046 *	0.174±0.041 *,†	0.177±0.043 *,†
aBV/TV	0.103±0.04	0.101±0.042	0.101±0.041	0.1±0.044	0.092±0.036 *,†	0.09±0.037 *,†
pBV/BV	0.329±0.117	0.322±0.124	0.319±0.122 *	0.313±0.131 *	0.307±0.116 *,†	0.301±0.121 *,†
rBV/BV	0.671±0.117	0.678±0.124	0.681±0.122 *	0.687±0.131 *	0.693±0.116 *,†	0.699±0.121 *,†
pTb.N (1/mm)	1.397±0.233	1.392±0.24	1.359±0.254 *	1.35±0.268 *	1.349±0.246 *,†	1.344±0.252 *
rTb.N (1/mm)	1.944±0.185	1.968±0.19	1.906±0.202 *	1.922±0.216 *	1.932±0.191 *,†	1.953±0.194 †
pTb.Th (mm)	0.213±0.009	0.212±0.01	0.214±0.01	0.214±0.009	0.207±0.008 *,†	0.206±0.007 *,†
rTb.Th (mm)	0.212±0.008	0.209±0.007	0.216±0.009 *	0.215±0.008 *	0.208±0.009 *,†	0.206±0.008 *,†
pTb.S (mm^2)	0.152±0.012	0.151±0.013	0.154±0.013 *	0.154±0.013 *	0.147±0.011 *,†	0.146±0.011 *,†
rTb.ℓ (mm)	0.648±0.034	0.646±0.033	0.656±0.041 *	0.654±0.043 *	0.645±0.034 †	0.643±0.034 †
R-R Junc.D ($1/mm^3$)	3.424±1.09	3.56±1.113	3.273±1.122 *	3.369±1.171 *	3.381±1.082 †	3.504±1.086 †

	Auto Contour S1	Auto Contour S2	Manual S1	Manual S2	Standard S1	Standard S2
R-P Junc.D (1/mm^3)	4.058±1.461	4.104±1.507	3.8±1.534 *	3.812±1.588 *	3.842±1.518 *	3.889±1.537 *
P-P Junc.D (1/mm^3)	1.953±0.807	1.959±0.834	1.826±0.84 *	1.826±0.875 *	1.803±0.795 *	1.807±0.818 *

* indicates significant difference from the measurements using the auto contour method;

† indicates significant difference from the manual contour method for the corresponding scans.

Table 3

RMSCV% of ITS parameters for radius and tibia, sub-categorized by image quality. G1 is the group with grade 1 quality for both scans, G2-4 is the group contains at least one scan categorized as quality grade 2, 3 or 4.

	Auto contour			Manual			Standard		
Tibia									
	Overall	G1	G2-4	Overall	G1	G2-4	Overall	G1	G2-4
BV/TV	1.7	1.3*	2.5	1.9	1.4*	2.7	1.8	1.3*	2.8
pBV/TV	5.2	3.7*	7.6	5.4	3.9*	7.7	5.5	3.7*	8.3
rBV/TV	7.9	4.7*	12.4	8	4.8*	12.7	7.6	4.7*	12
aBV/TV	5.6	3.8*	8.4	5.7	4*	8.5	5.6	3.9*	8.3
pBV/BV	6.5	4.4*	9.8	6.6	4.4*	10.1	7	4.5*	10.7
rBV/BV	6.5	3.8*	10.2	6.5	3.9*	10.3	6.1	3.7*	9.5
pTb.N	0.9	0.9	1	1†	1	1.1	1	0.9	1.1
rTb.N	3.6	2.4*	5.6	3.8†	2.5*	5.8	3.5††	2.3*	5.4
pTb.Th	0.6	0.5	0.8	0.6	0.5*	0.8	0.7	0.4*	1.1
rTb.Th	1.7	1.4	2.2	1.8†	1.5	2.4	1.6††	1.3	2
pTb.S	3.4	2.1*	5.2	3.4	2.2*	5.3	3.1	2.1*	4.7
rTb.ℓ	0.8	0.4*	1.2	0.8	0.5*	1.2	0.8	0.4*	1.3
R-R Junc.D	13.4	8.4*	20.9	13.9	8.6*	21.8	12.8††	8.1*	19.9
R-P Junc.D	5.9	4*	8.8	6.1	4.3*	9	5.6††	4.1*	8
P-P Junc.D	2.3	2.3	2.4	2.6	2.6	2.7	2.4	2.5	2.1
Radius									
BV/TV	2.1	2.1	2.1	2.7	1	3	2.7	2.6	3.1
pBV/TV	9	4.2	10	10.2	4.3	11.4	9.2	4.9	10.1
rBV/TV	7.3	5	7.8	7.1	2.1*	8	7.1	5.6	7.5
aBV/TV	8.3	4.8	9.2	8.1	2.1*	9.2	7.4	6.6	7.7
pBV/BV	9.7	5.2	10.7	10.1	4.1*	11.3	10	6.3	10.9
rBV/BV	6.2	3.2	6.9	6.1	1.8	6.9	5.5	3.1	6.1
pTb.N	2.3	0.9	2.6	3.1	1.3	3.5	2.6	2	2.8
rTb.N	3.5	3.2	3.6	3.4	1.5	3.8	3.6	3.5	4
pTb.Th	1.2	0.9	1.3	1.5	0.4*	1.7	1.6	1.7	1.6
rTb.Th	2	1.8	2.5	2	1.4	2.1	2.4	2*	3.5
pTb.S	3.1	2.4	3.3	3	1*	3.4	3	2.6	3.1
rTb.ℓ	0.9	0.5	1	0.9	0.8	0.9	1	0.9	1.1
R-R Junc.D	12.3	10.3	12.8	11.7	4.4	13.1	12.2	11.9	12.3

	Auto contour			Manual			Standard		
R-P Junc.D	6.4	5.9	6.6	7.4	2.6*	8.4	7.7	8.7	7.4
P-P Junc.D	5.8	2.9	6.5	7.7	3.8	8.6	7.1	6.2	7.3

* indicates significant difference from G2-4 group ($p<0.05$) within each group;

† indicates significant difference from the auto contour method ($p<0.05$),

†† indicates significant difference from the manual contour method ($p<0.05$).

Table 4

Least significant detectable change for quantitative ITS measures.

	Tibia			Radius		
	Auto	Manual	Standard	Auto	Manual	Standard
BV/TV	0.015	0.016	0.015	0.016	0.021	0.019
pBV/TV	0.02	0.02	0.018	0.024	0.026	0.021
rBV/TV	0.038	0.038	0.036	0.037	0.036	0.034
aBV/TV	0.02	0.02	0.018	0.024	0.023	0.019
pBV/BV	0.079	0.079	0.079	0.088	0.089	0.085
rBV/BV	0.101	0.103	0.1	0.116	0.115	0.107
pTb.N	0.039	0.043†	0.041	0.09	0.117	0.099
rTb.N	0.192	0.199†	0.188††	0.191	0.18	0.195
pTb.Th	0.004	0.004	0.004	0.007	0.009	0.009
rTb.Th	0.01	0.011†	0.009††	0.012	0.012	0.014
pTb.S	0.015	0.015	0.013	0.013	0.013	0.012
rTb.ℓ	0.013	0.014	0.014	0.016	0.016	0.018
R-R Junc.D	1.151	1.175	1.13††	1.164	1.059	1.145
R-P Junc.D	0.729	0.736	0.697††	0.721	0.782	0.821
P-P Junc.D	0.153	0.17	0.153	0.316	0.391	0.352

† indicates significant difference from the auto contour method ($p<0.05$),

†† indicates significant difference from the manual contour method for overall data ($p<0.05$).